FRONT SIDE STRUCTURES IN TIO₂ FOR CRYSTALLINE SILICON SOLAR CELLS: WHICH EFFECTS CAN THEY ACHIEVE?

L. Stevens[1], H. Hauser[1], O. Höhn[1], N. Tucher[1,2], C. Wellens[1], C. Stauch[3], R. Jahn[3], C. Müller[4], B. Bläsi[1]

[1] Fraunhofer ISE, Heidenhofstraße 2, 79110 Freiburg, Germany
[2] University Freiburg, INATECH, Georges-Köhler-Allee 103, 79110 Freiburg, Germany
[3] Fraunhofer ISC, Neunerplatz 2, 97082 Würzburg, Germany
[4] University Freiburg, IMTEK, Georges-Köhler-Allee 103, 79110 Freiburg, Germany

ABSTRACT

Light trapping and reflection reduction are essential, in order to enhance the absorption of silicon solar cells. State of the art in industry is texturization using wet chemical etching of the front surface in combination with the deposition of antireflection coatings to improve the solar cell optics. Within this work an alternative route, namely a TiO₂ coating with nano structures on the front side of a planar silicon solar cell encapsulated in ethylene vinyl acetate (EVA) and glass, is analyzed. The focus is put on the experimental realization of such a system. Optical measurements are compared to optical simulations using the rigorous coupled wave analysis (RCWA) and the OPTOS method. Good agreement between measurements and simulation was found, so the simulation modell can be used in the future for prediction of the optical perfomance of different structures even in a PV-module.

1 INTRODUCTION

Strong light coupling into solar cells as well as good light trapping is important to maximize the energy conversion efficiency. To improve these optical properties, a surface texturing with an antireflection coating is typically applied in silicon photovoltaics [1]. The standard process for texturing in industry is wet chemical etching, which produces a random pyramidal structure for monocrystalline silicon [2] and the so-called isotexture for multicrystalline silicon [3]. All etching processes lead to an enlargement of the surface area, which leads to increased surface recombination.

An alternative approach, based on the patterning of a high index TiO₂ sol-gel was introduced by Spinelli et al.[4]. Using this approach, a surface enlargement can be avoided as an optically functional surface is additively applied onto a planar electrically passivated surface.

We also investigated inorganic sol-gel materials as they feature a high refractive index to fulfil the desired optical functionality of efficient light incoupling [5–7]. Furthermore they can be patterned via nanoimprint lithography (NIL) [8]. This process in principle offers higher degree of freedom concerning the structure profile compared to the etching processes.

In contrast to the work of Spinelli et al [9], we designed our surface structures in order to optimise the optical performance for solar cells being encapsulated in a PV module (i.e. total internal reflection within the module glass) [10], which in the end is the relevant case for application. In the present work we realized patterned TiO₂ layers by means of NIL and characterized the samples optically in the following stages (1) bare silicon wafer with TiO₂ AR structure, (2) with additional Ag rear side mirror and (3) additionally encapsulated in a module. Optical measurements and corresponding simulations for these different stages show good agreement. The simulations in this case study were performed using OPTOS (optical properties of textured optical sheets) [11–13], a matrix based approach to incoherently couple textured interfaces of arbitrary spatial regime. Thus, best suited methods can be applied to model solely the textured interface, which in our case was done using the rigorous coupled wave analysis (RCWA) [14].

2 EXPERIMENTAL

With the experimental realization we aimed for a structure with similar properties as presented in [10], which is a height of 110 nm, a period of 600 nm and a geometric filling factor of 0.275. The latter is defined as the ratio of the area consisting of TiO₂ pillars (A_{TiO2}) to the area of the simulated unit cell of the structure ($A_{unitcell}$). A sketch of the targeted structure is shown in Fig. **1**.
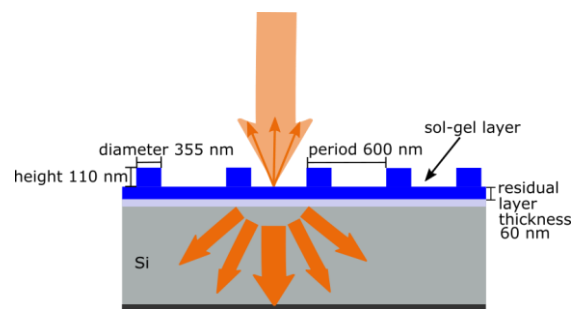

Fig. 1: Sketch of the targeted structure with a height of 110 nm, a diameter of 355 nm, a period of 600 nm and a residual layer thickness of 60nm.

2.1 Experimental realization of the structure

We experimentally realized binary TiO₂ structures on silicon with parameters preferably close to the design parameters. The process starts with a master structure generated with interference lithography [15,16] which is replicated into a polydimethylsiloxane (PDMS) material.

The process chain is presented in Fig. 2. After applying the TiO₂ precursor dissolved in a mixture of ethanol and 1,5-pentanediol on the silicon wafer, a following softbake step is done. This is necessary to evaporate the lower volatile solvent. A PDMS stamp is then used in a NIL pro-

cess to structure the material. Radiation process helps to evaporate more solvent into the stamp and harden the structure. To achieve a higher refractive index, the sol-gel structure is finally sintered after the imprint process. The sintering undergoes large shrinkage (in our case 70 %). A detailed description including all process parameters can be found in [17].
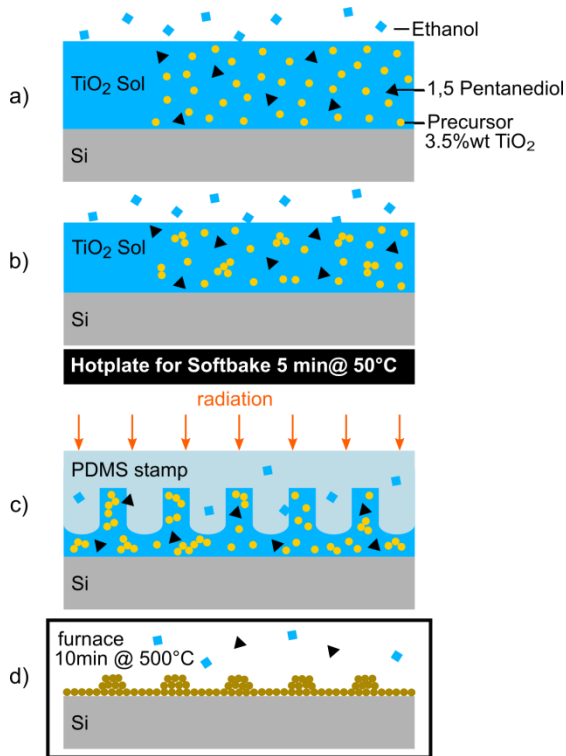

Fig. 2: Description of the process chain. In a) is the application of the sol-gel material consisting of the solvents ethanol and 1,5-pentanediol and the precursor TiO_2 via spin coating presented. b) shows the softbake step to evaporate the lower volatile solvent . The following step (c) is the structuring with a PDMS stamp by using radiation. The stamp absorbs ethanol, so the structure is getting harder. To increase the refractive index and evaporate all organic solvents, the last step is the sintering in a furnance (d)).

The resulting structure parameters were characterized with a Bruker Dimension Edge atomic force microscope (AFM) (see Fig. 3). The structure depth of around 50 nm and a period of around 590 nm could be determined. Also the filling factor was calculated from the AFM image to be 0.75.
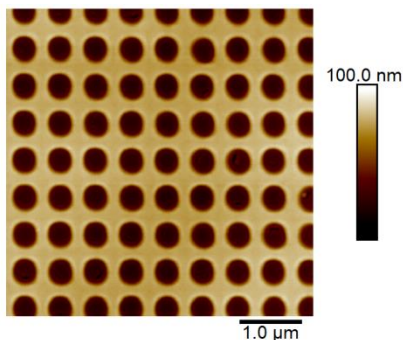

Fig. 3: AFM image in top view position of the structure. The structure depth was determined to be around 50 nm and the period is around 590 nm. The smaller period compared to the design period is due to the sintering process.

The residual layer thickness was determined with a scanning electron microscope (SEM) to be around 60 nm (see Fig. 4).
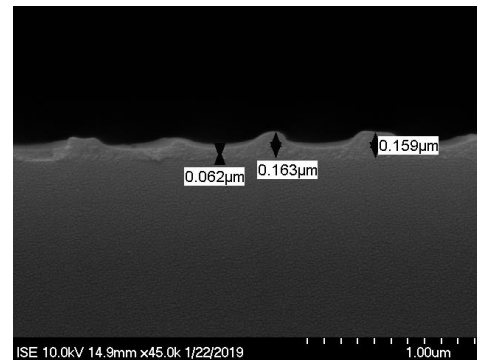

Fig. 4: SEM micrographs of the realized sol-gel structure. In the picture the cross section of the structure is shown. Due to procedural reasons the imprinted structures have holes and not pillars. The residual layer thickness is determined to be around 60 nm, the structure height with around 100 nm.

The hole-structure was optically analyzed in three different cases (see Fig. 5).

- Case 1: Structure on a bare silicon wafer
- Case 2: Structure on a silicon wafer with silver rear side mirror
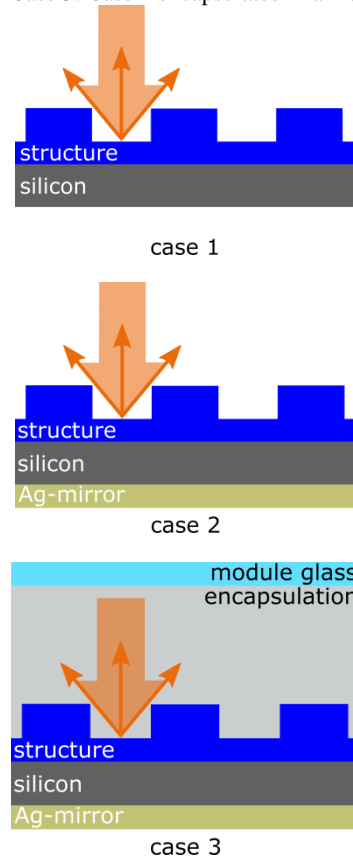- Case 3: Case 2 encapsulated in a module

Fig. 5: Sketch of the three different experimentally realized cases of a TiO_2 structured sol-gel layer on top of a silicon wafer (wafer thickness: 200 µm, sketch not to scale). Case 1 represents a structured TiO_2 layer on silicon, case 2 has an additional Ag-mirror at the backside and case 3 is a structured TiO_2 layer on silicon with Ag-mirror at the backside in a module encapsulation.

In order to determine the reflectance of the experimentally realized structure the samples were measured with the help of a Fourier spectrometer. Fig. 6 shows reflectance measurements of case 1, a Si-Wafer with structured TiO_2 layer (black), of case 2, a Si-Wafer with an Ag-backside and a structured TiO_2 layer at the front side (red) and case 3, a Si-Wafer with structured TiO_2 layer in a module encapsulation (green). The curves of the structured layer with and without Ag-backside show the same behavior for wavelengths below 960 nm. The different reflectance above 960 nm is due to the existence of the Ag-backsides. When including a module encapsulation, the reflectance increases in the minimum and decreases a bit in the maximum. The reason is the additional reflection at the module frontside and the refractive index of the surrounding of approx. 1.5, which is higher than the refractive index of the surrounding air (n=1). The dip of the curve around a wavelength of 1200 nm is caused by absorption in the encapsulation material EVA of the module.
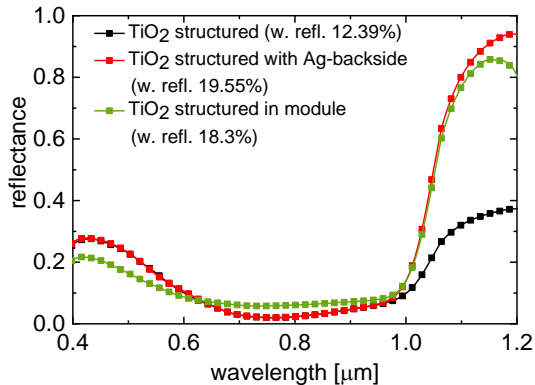

Fig. 6: Measured optical results of a structured area each in the three different cases. Weighted reflection calculated from Am1.5g spectrum weighted in the wavelength range from 400-1200 nm.

2.2 Comparing experimental results with optical simulations

The samples were modelled wave optically, using the experimentally determined structure parameters as input parameters. The results are shown in Fig. 8. As in these simulations only the RCWA approach was applied, we modelled semi-infinite silicon wafers for the sake of simplicity. In the first approximation a binary hole structure was simulated. In black points the measured experimental data is shown. To exclude the reflection at the wafer rear side and thus be comparable to simulations of infinitely thick substrates, this measurement was linearly extrapolated beyond 950 nm shown in grey points.

In a first step binary holes with a structure height of 33 nm, a residual layer thickness of 60 nm and period of 586 nm were modelled (shown in red). A good agreement with measured data for wavelengths above 580 nm can be seen. Below this wavelength, the simulated reflectance is too high. When comparing the used parameter from the simulation to measured parameters it attracts attention, that the modeled height of 33 nm is quite smaller than the measured. This is due to the fact, that a binary profile with similar optical functions as a continous profil typically needs a smaller depth [18].

In order to find a better fitting structure model, the filling factor distribution over the structure height was determined from an AFM image and a step function was fitted to that distribution with eight steps (see Fig. 7).
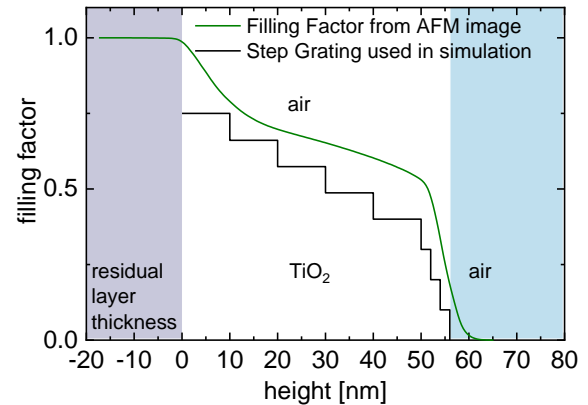

Fig. 7: From the AFM image determined filling factor and the used step function from the simulation..

Using the step grating with the parameter combination of a height of 56 nm, a period of 586 nm, a area filling factor of 0.75 and a residual layer thickness of 50 nm (shown as blue curve), the simulation and the measurement data fit very well together. 10 nm differences in the residual layer thickness compared to the value determined via SEM are within the measurement accuracy as the hight measurement with SEM is not calibrated and there are also height differences over the imprinted area that were not systematically analyzed. In summary, we could find a structure model, which describes the measurement data very well.
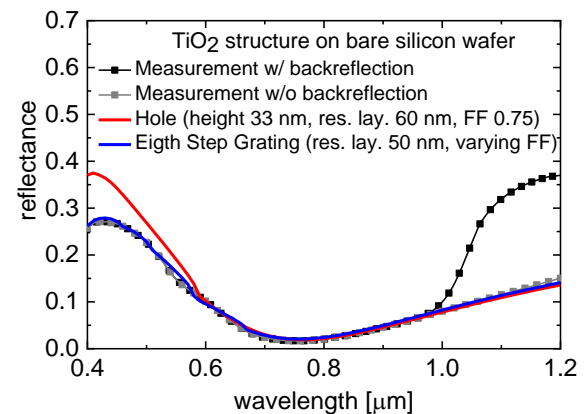

Fig. 8: Results of the comparison between experimental and simulation data for the structure measured in air without Ag mirror. The reflection measurement shown in black includes also the backside reflection of the wafer. For a comparison with the simulation data only the front side reflectance was determined from the experimental data shown in grey points. In red the simulation results of a pillar filled with air surrounded by TiO_2 is presented. In blue is the result of a step function with eight steps and a residual layer of 50 nm presented.

Using this step grating, Fig. 9 shows as a result of the case 2, a Si-Wafer with an Ag-backside, the comparison of the measurement result (red points) and an OPTOS simulation data (purple), which are also in very good agreement. This leads to the conclusion, that the RCWA simulation in combination with the OPTOS method can

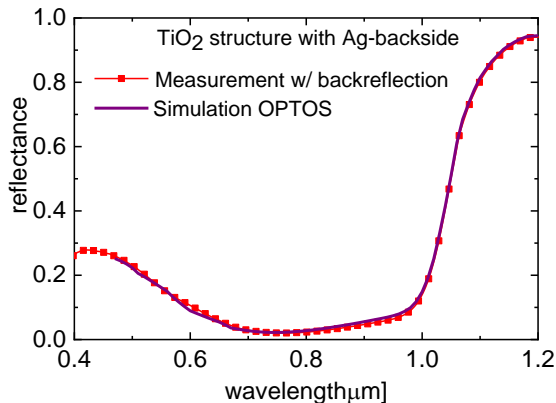be used to predict the reflectance of a sol-gel structure very well.

Fig. 9: Comparison of the measured results of the case 2 and the simulation using the step function with a residual layer thickness of 50 nm within the OPTOS method.

Comparing the measurement results (dark green) of case 3 (see Fig. 10) with OPTOS simulation (dark red) a very good agreement could be shown too. In the wavelength range above 1000 nm the simulation overestimated the reflection compared to the measurement. This is most likely due to underestimation of the absorbance in the EVA. In order to assess the optical influence of a structure compared to an eight-layer stack, the reflections of these two systems were compared. For this purpose, effective refractive indexes based on the filling factor distribution of the step function were used for the eight-layer stack in the transfer–matrix-method [19] (shown in orange). It was found that the reflectance of the structure is higher than that of an eight-layer planar antireflection system. For relevant light trapping, the reflection of the structured layer in the long-wavelength range would have to be significantly lower compared to the eight-layer stack. But as it is visible in Fig. 10 the reflections in the long wavelength range for both systems are similar. This points out that the experimentally realized structure does not cause any relevant light trapping in the structure.
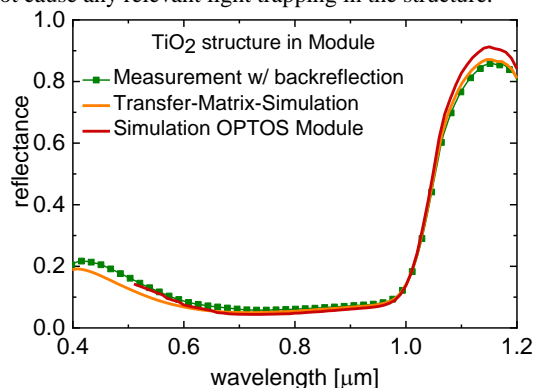

Fig. 10: Comparison of the measurement and simulation results for the module case. The simulation data (red) are in very good agreement with the measurement data (green). To check if there is relevant light trapping in the TiO_2 structure a transfer-matrix-method was used for an eight-layer planar antireflection coating system. The reflectance of that system is in the lower wavelength range smaller than that of the structured TiO_2 layer and in the higher wavelength ranges similar.

Although no light trapping could be shown experimentally, the very good agreement of the OPTOS simulation to the measurements confirms the accuracy of the simulation model for such complex systems. Thus, it can be used in the future for an accurate prediction of the optical performance of different structures even in a PV-module.

4 CONCLUSION

We used NIL to imprint a TiO_2 based sol-gel in order to avoid surface enlargement by structuring the silicon solar cell surface. Nanometer structures were realized experimentally. Optical measurements were compared to wave optical simulations using the RCWA and the OPTOS method.

The OPTOS simulation method showed a very high precision in prediction to experimental data for all investigated systems (solar cells as well as solar modules). Thus, this model can be used in future for a reliable optical analysis of different structures.

With the help of transfer-matrix-simulation and comparisons to the full OPTOS modeling it could be shown that the analyzed structure does not lead to relevant light trapping.

5 ACKNOWLEDGEMENTS

6 REFERNCES

1. M. A. Green, *High efficiency silicon solar cells* (Trans Tech Publications, 1987).
2. P. Campbell and M. A. Green, "Light trapping properties of pyramidally textured surfaces," J. Appl. Phys. **62**, 243 (1987).
3. A. Hauser, I. Melnyk, P. Fath, S. Narayanan, S. Roberts, and T. M. Bruton, "A simplified process for isotropic texturing of mc-Si," in *Proceedings of the 3rd World Conference on Photovoltaic Energy Conversion* (2003), pp. 1447–1450.
4. P. Spinelli, B. Macco, M. A. Verschuuren, Kessels, W. M. M., and A. Polman, "Al2O3/TiO2 nano-pattern antireflection coating with ultralow surface recombination," Appl. Phys. Lett. **102**, 233902 (2013).
5. M. Bockmeyer and P. Löbmann, "Crack formation in TiO2 films prepared by sol–gel processing: Quantification and characterization," Thin solid films **515**, 5212–5219 (2007).
6. P. Löbmann, "Soluble Powders as Precursors for TiO2 Thin Films," Journal of Sol-Gel Science and Technology **33**, 275–282 (2005).
7. P. Löbmann, R. Jahn, S. Seifert, and D. Sporn, "Inorganic Thin Films Prepared from Soluble Powders and Their Applications," Journal of Sol-Gel Science and Technology **19**, 473–477 (2000).
8. C. Peroz, V. Chauveau, E. Barthel, and E. Søndergård, "Nanoimprint lithography on silica sol-gels: a simple route to sequential patterning," Advanced materials (Deerfield Beach, Fla.) **21**, 555–558 (2009).

9. P. Spinelli, M. A. Verschuuren, and A. Polman, "Broadband omnidirectional antireflection coating based on subwavelength surface Mie resonators," Nature communications **3**, 692 (2012).

10. L. Stevens, N. Tucher, O. Höhn, H. Hauser, C. Müller, and B. Bläsi, "Broadband antireflection Mie scatterers revisited—a solar cell and module analysis," Opt. Express **27**, A524 (2019).

11. N. Tucher, J. Eisenlohr, H. Gebrewold, P. Kiefel, O. Höhn, H. Hauser, J. C. Goldschmidt, and B. Bläsi, "Optical simulation of photovoltaic modules with multiple textured interfaces using the matrix-based formalism OPTOS," Optics Express **24**, A1083 (2016).

12. N. Tucher, J. Eisenlohr, P. Kiefel, O. Höhn, H. Hauser, I. M. Peters, C. Müller, J. C. Goldschmidt, and B. Bläsi, "3D optical simulation formalism OPTOS for textured silicon solar cells," Opt. Express **23**, A1720 (2015).

13. N. Tucher, J. Eisenlohr, P. Kiefel, O. Höhn, H. Hauser, I. M. Peters, C. Müller, J. C. Goldschmidt, and B. Bläsi, "Optical properties of textured sheets: an efficient matrix-based modelling approach," in *Proc. of SPIE*, Vol. 9630 of Proceedings of SPIE (SPIE, 2015), p. 96300.

14. M. G. Moharam and T. K. Gaylord, "Diffraction analysis of dielectric surface-relief gratings," J. Opt. Soc. Am. **72**, 1385–1392 (1982).

15. A. J. Wolf, H. Hauser, V. Kübler, C. Walk, O. Höhn, and B. Bläsi, "Origination of nano- and microstructures on large areas by interference lithography," Microelectron Eng **98**, 293–296 (2012).

16. B. Bläsi, H. Hauser, O. Höhn, V. Kübler, I. M. Peters, and A. J. Wolf, "Photon management structures originated by interference lithography," in *Proceedings of the 1st International Conference on Crystalline Silicon Photovoltaics (SiliconPV)* (Elsevier, 2011), pp. 712–718.

17. L. Stevens, H. Hauser, O. Höhn, N. Tucher, C. Wellens, R. Jahn, W. Glaubitt, C. Müller, and B. Bläsi, "Nanoimprinted sol-gel materials for antireflective structures on silicon solar cells," in *Proc. SPIE 10688, Photonics for Solar Energy Systems VII, 106880B (22 May 2018)* , p. 10.

18. B. Bläsi, *Holographisch hergestellte Antireflexoberflachen fur solare und visuelle Anwendungen*, Dissertation, Universität Freiburg, 2000.

19. Bruggeman, D. A. G., "Berechnung verschiedener physikalischer Konstanten von heterogenen Substanzen. I. Dielektrizitätskonstanten und Leitfähigkeiten der Mischkörper aus isotropen Substanzen," Annalen der Physik **416**, 636–664 (1935).